

Statistical features of quantum chaos using the Krylov operator complexity

Zhuoran Li and Wei Fan ¹

Department of Physics, School of Science, Jiangsu University of Science and Technology, Zhenjiang, 212100, China

E-mail: zrl2l2r@gmail.com, fanwei@just.edu.cn

ABSTRACT: Recently the variance of Lanczos coefficients in the Krylov space of an initial operator is recognized as an important indicator of quantum chaos. In this paper, we generate samples of random initial operators from given probability distributions (GOE, GUE and the uniform distribution) and do statistics on the variance of Lanczos coefficients over these initial operators. Using the Sinai billiard with an integrability-breaking term, we propose two statistical quantities that have distinct behaviors as the system changes from nonchaotic to chaotic. One is the average correlation matrix $\langle x_i x_j \rangle$ of Lanczos coefficients, which exhibits different patterns in the nonchaotic and the chaotic regime. The other one is the resulting distribution of the variance of Lanczos coefficients. In the nonchaotic case, the resulting distributions are almost overlapping together. In the chaotic case, they split into two well-separated groups. Furthermore, the resulting statistics of these two quantities are the Wishart distribution and the (rescaled) chi-square distribution respectively, which are independent of the distributions of initial operators and become the normal distribution in the case of large matrix size.

¹Corresponding author.

Contents

1	Introduction	1
2	Preliminary: Krylov operator space	3
3	Statistical properties of Lanczos coefficients	5
3.1	Intuition on the normal distribution	6
3.2	Distribution of the average correlation matrix $\langle x_i x_j \rangle$	7
3.3	Distribution f_{σ^2} of the variance σ^2	9
4	Model and Results	10
5	Discussion	12
A	Check the normal distribution of σ^2 for $\mathcal{N}_{max} = 100$	15
B	Different choice of algorithm step sizes for b_n	16
C	Check the chi-square distribution of σ^2 for $\mathcal{N}_{max} = 5$	17

1 Introduction

The physics of complexity is important for understanding many different phenomena, ranging from condensed matter physics to black hole physics. Especially, the operator complexity captures the spread of an operator under time evolution and is an important indicator in the analysis of chaos. Recently the spread of an operator is explored in the Krylov space [1], where the dynamics depends on the expansion coefficients of the operator in the Krylov basis and on the Lanczos coefficients generated in the process of constructing this Krylov basis. The Krylov complexity (K-complexity) [1] constructed from the expansion coefficients is proposed as an upper bound on the operator complexity, including the famous bound $\lambda_L \leq 2\pi k_B T / \hbar$ [2] of the growth of the out-of-time-order correlation function (OTOC) [3].

Interestingly, the operator dynamics in the Krylov space resembles the hopping dynamics on a 1d chain [1], called the Krylov chain, with the hopping amplitudes being the Lanczos coefficients. Using this analog, the erratic behavior of Lanczos coefficients is analyzed [4, 5] in terms of the Anderson localization. The variance σ^2 of Lanczos coefficients is introduced [5] to explain the suppression of the late-time saturation value of K-complexity in the integrable XXZ spin chain. This suggests that the variance σ^2 of Lanczos coefficients may play an important role in distinguishing chaotic and nonchaotic behaviors.

Then it leads to an interesting connection between K-complexity and Random Matrix Theory (RMT). By adding an integrability-breaking term to the XXZ spin chain, the late-time saturation value of K-complexity is computed as the system changes from nonchaotic to chaotic behavior [6]. It approaches the behavior of similar values computed with Hamiltonian drawn from RMT ensembles [6]. Also, three different initial operators generating the Krylov space is randomly selected and compared there [6]. In [7], the K-complexity is also studied by choosing multiple initial operators.

Furthermore, a statistical correlation between the variance σ^2 of Lanczos coefficients and the level statistics [8–12] is reported in the billiard systems [13]. As the system Hamiltonian varies from nonchaotic to chaotic, the variance σ^2 of Lanczos coefficients is computed for an initial momentum operator and the level statistics are computed as usual. The linear correlation coefficient between these two sequences of data are not zero.

Along this line, an important question arises: *what would happen for the Lanczos coefficients if we do statistics of initial operators over a given probability distribution.* In this paper, we study this possibility by generating samples of initial operators from a given probability distribution (GOE, GUE and the uniform distribution) and analyzing the resulting Lanczos coefficients. Interestingly, we find two statistical quantities that behave distinctively in the nonchaotic and the chaotic regime after averaging over the sample. One is the average correlation matrix $\langle x_i x_j \rangle$ of Lanczos coefficients. In the nonchaotic regime, it has a pattern that locally resembles the two-electron wave function of the Anderson localization [14], but this pattern disappears (or fading away by spreading out uniformly) in the chaotic regime. The other one is the resulting distribution of the variance σ^2 . For samples of initial operators from different distributions, the resulting distributions of σ^2 are nearly the same in the nonchaotic case, but split into two well-separated groups in the chaotic case. Intuitively, the resulting plots of distributions of σ^2 are overlapped together in the nonchaotic case, and divide into two well-separated groups in the chaotic case. Furthermore, we find that the average correlation matrix $\langle x_i x_j \rangle$ satisfies the Wishart distribution and the resulting distribution of σ^2 satisfies a rescaled chi-square distribution. This is independent of the initial operator distributions and approaches the normal distribution as the size of the operator matrix increases.

In detail, we consider the Sinai billiard, which is a typical billiard system originating from a quantization of classical chaos [15]. The numerical computation is done in the energy representation and operators become matrices. Each time, a random initial operator \mathcal{O} is sampled out by picking the corresponding random matrix from the following distributions: the GOE, the GUE, the uniform distribution of complex numbers (UCP), the uniform distribution of pure real numbers (URE) and of pure imaginary numbers (UIM). Then the Lanczos coefficients are computed in the Krylov space associated with this operator, which give the correlation matrix $x_i x_j$ and the variance σ^2 of Lanczos coefficients. Repeating this enough times, the average correlation matrix $\langle x_i x_j \rangle$ and the distribution of the variance σ^2 can be extracted for different samples of initial operators. Finally, these two statistical quantities are computed as the system changes from nonchaotic to chaotic. Independent of the initial distributions, the resulting statistics of $\langle x_i x_j \rangle$ and of σ^2 approach the normal distribution when the size of matrix becomes large, as discussed in Section 3. For the

average correlation matrix $\langle x_i x_j \rangle$, its different patterns in the nonchaotic and the chaotic regime are shown in Figure 5. For the resulting normal distributions of σ^2 , the logarithm of its statistical average $\langle \sigma^2 \rangle$ and standard deviation are shown in Figure 8. In the nonchaotic case, the resulting distributions of σ^2 are almost overlapping together for all the five initial distributions. In the chaotic case, they split into two groups well-separated from each other: one group consists of GOE, URE and UIM, while the other group consists of GUE and UCP.

The paper is organized as follows. In Section 2, we briefly review the relevant physics of the Krylov operator space and explain the sampling of random initial operators. In Section 3, we qualitatively explain the Wishart distribution of $\langle x_i x_j \rangle$ and the chi-square distribution of σ^2 , which approach the normal distribution when the size of matrix is large enough. In Section 4, we show the detailed results for the Sinai billiard. In Section 5, we discuss the physics of our results and conclude with a discussion of open questions.

2 Preliminary: Krylov operator space

Here we briefly review the algorithms of Krylov operator space [1]. Readers familiar with it can skip this section. For a quantum system with the Hamiltonian H , the time evolution of a given operator \mathcal{O} in the Heisenberg picture is given by

$$\mathcal{O}(t) = e^{iHt} \mathcal{O}(0) e^{-iHt} \quad (2.1)$$

Using the Baker-Campbell-Hausdorff formula, it can be expanded as

$$\mathcal{O}(t) = \sum_{n=0}^{\infty} \frac{(it)^n}{n!} \mathcal{L}^n \mathcal{O}(0), \quad (2.2)$$

where $\mathcal{L} := [H, \cdot]$ is the Liouvillian superoperator. This sequence of operators $\mathcal{O}(0)$, $\mathcal{L}\mathcal{O}(0)$, $\mathcal{L}^2\mathcal{O}(0)$, \dots spans a space associated with the operator $\mathcal{O}(0)$. This space is the Krylov subspace generated by \mathcal{L} (and hence H) and $\mathcal{O}(0)$, that is,

$$\mathcal{K}_m(\mathcal{L}, \mathcal{O}(0)) \equiv \{\mathcal{O}(0), \mathcal{L}\mathcal{O}(0), \mathcal{L}^2\mathcal{O}(0), \dots, \mathcal{L}^m\mathcal{O}(0)\} \quad (2.3)$$

An orthonormal basis, called the Krylov basis, can be constructed for $\mathcal{K}_m(\mathcal{L}, \mathcal{O}(0))$. This construction also generates a sequence of important numbers called the Lanczos coefficients, because the algorithm used is the Lanczos algorithm (or similar algorithms). The orthogonality is guaranteed by the inner product $(A|B) = \text{tr}[A^\dagger B]$, which can be considered as a simplification of the Wightman inner product at infinite temperature. The Lanczos algorithm can be briefly stated as follows:

Require: $\|\mathcal{O}\| = \sqrt{(\mathcal{O}|\mathcal{O})}$

- 1: $b_0 \leftarrow 0$
- 2: $\mathcal{O}_{-1} \leftarrow 0$
- 3: $\mathcal{O}_0 \leftarrow \mathcal{O}(0)/\|\mathcal{O}(0)\|$
- 4: $n \leftarrow 1$
- 5: **while** $b_n \neq 0$ **do**
- 6: $\mathcal{A}_n \leftarrow \mathcal{L}\mathcal{O}_{n-1} - b_{n-1}\mathcal{O}_{n-2}$

7: $b_n \leftarrow \|\mathcal{A}_n\|$
8: $\mathcal{O}_n \leftarrow \mathcal{A}_n/b_n$
9: $n \leftarrow n + 1$
10: **end while**

The Krylov basis is given by $\{|O_0\rangle, |O_1\rangle, \dots, |O_{n_k-1}\rangle\}$ and the dimension of Krylov operator space is $n_k = \dim(\mathcal{K}_m)$. The sequence of positive numbers $\{b_n\}$ is called the Lanczos coefficient and is essentially the matrix element of the Liouvillian operator

$$L_{nm} \equiv (\mathcal{O}_n | \mathcal{L} | \mathcal{O}_m) = \begin{pmatrix} 0 & b_1 & 0 & 0 & \cdots \\ b_1 & 0 & b_2 & 0 & \cdots \\ 0 & b_2 & 0 & b_3 & \cdots \\ 0 & 0 & b_3 & 0 & \cdots \\ \vdots & \vdots & \vdots & \cdots & \cdots \end{pmatrix} \quad (2.4)$$

The Lanczos coefficient $\{b_n\}$ is essential for the evolution of the operator $\mathcal{O}(t)$. To see this, firstly expand the operator $\mathcal{O}(t)$ in terms of the Krylov basis

$$\mathcal{O}(t) = \sum_{n=0}^{n_k-1} i^n \varphi_n(t) \mathcal{O}_n, \quad \varphi_n(t) \equiv (\mathcal{O}_n | \mathcal{O}(t)) / i^n, \quad (2.5)$$

and then substitute it into the Heisenberg equation, which leads to the following equation

$$\dot{\varphi}_n(t) = b_n \varphi_{n-1}(t) - b_{n+1} \varphi_{n+1}(t), \quad (2.6)$$

with the dot being the time derivative and the initial condition being $\varphi_n(0) = \delta_{n0} \|\mathcal{O}\|$. This equation suggests that the spreading behavior of an operator in the Krylov space resembles the dynamics of wave functions on a 1d chain, called the Krylov chain [1], where $\varphi_n(t)$ is the wave function and b_n is the hopping amplitude. This makes it possible to connect the operator complexity in the Krylov space with condensed matter physics on spin chains. The tridiagonal form of the Liouvillian operator is another feature of the Krylov chain. On this Krylov chain, the time-dependent average position acts naturally as an indicator of the spreading behavior and is defined as the K-complexity

$$C_K(t) = \sum_{n=0}^{n_k-1} n |\phi_n(t)|^2. \quad (2.7)$$

The K-complexity has been playing an important role in the analysis of quantum chaos, see the review [16] for related works.

Obviously, results in the Krylov space will vary when the initial operator \mathcal{O} changes. One way to deal with this dependence on initial operators is to do statistics and this is what we do in this paper. We choose samples of random initial operators from different probability distributions and study the resulting statistics of the Lanczos coefficients. Specifically, we consider random initial operators (\mathcal{O}_{GOE} , \mathcal{O}_{GUE} and \mathcal{O}_{uni}) from the Gaussian orthogonal ensemble (GOE), the Gaussian unitary ensemble (GUE) and the uniform distribution.

These operators are evaluated in the energy representation. In the case of GOE, the random matrix, $\mathcal{O}_{mn} := \langle m | \mathcal{O}_{GOE} | n \rangle$, is a real symmetric matrix whose matrix elements satisfy the following joint probability density function [17]:

$$P(\mathcal{O}_{11}, \mathcal{O}_{12}, \dots, \mathcal{O}_{NN}) = \left(\frac{1}{2\pi}\right)^{\frac{N}{2}} \left(\frac{1}{\pi}\right)^{\frac{N^2-N}{2}} \exp\left[-\frac{1}{2}\text{Tr}(\mathcal{O}_{GOE}^2)\right]. \quad (2.8)$$

In the case of GUE, the random matrix, $\mathcal{O}_{mn}^{GUE} := \langle m | \mathcal{O}_{GUE} | n \rangle$ is Hermitian whose elements satisfy the following joint probability density function:

$$\begin{aligned} P(\mathcal{O}_{11}^{(0)}, \mathcal{O}_{12}^{(0)}, \dots, \mathcal{O}_{NN}^{(0)}) &= \left(\frac{1}{2\pi}\right)^{\frac{N}{2}} \left(\frac{1}{\pi}\right)^{\frac{N^2-N}{2}} \exp\left[-\frac{1}{2}\text{Tr}(\mathcal{O}^{(0)2})\right], \\ P(\mathcal{O}_{11}^{(1)}, \mathcal{O}_{12}^{(1)}, \dots, \mathcal{O}_{NN}^{(1)}) &= \left(\frac{1}{2\pi}\right)^{\frac{N}{2}} \left(\frac{1}{\pi}\right)^{\frac{N^2-N}{2}} \exp\left[-\frac{1}{2}\text{Tr}(\mathcal{O}^{(1)2})\right], \end{aligned} \quad (2.9)$$

with $\mathcal{O}^{(0)}$ being the real part of \mathcal{O}_{mn}^{GUE} , and $\mathcal{O}^{(1)}$ being the imaginary part of \mathcal{O}_{mn}^{GUE} . In the case of uniform distribution, three types of random operators are studied. Their random matrices belong to three types: purely real symmetric (URE), purely imaginary Hermitian (UIM), and complex Hermitian (UCP).

$$\mathcal{O}_{mn}^{(0,1)} \sim U(-\sqrt{3}, \sqrt{3}) \quad (2.10)$$

3 Statistical properties of Lanczos coefficients

The perspective of the Krylov chain (2.6) provides an efficient way to analyze the spreading dynamics of an operator by connecting to the physics of quantum many-body systems. Firstly in [18], the delocalization on the chain is proposed as the reason for the chaotic behavior of an operator on the many-body systems. Then in [5], the localization on the Krylov chain is proposed as the reason for the nonchaotic behavior of an operator on the XXZ spin chain.

Here, the Lanczos coefficients plays an an essential role because it is the hopping amplitude on the Krylov chain. The sequence of Lanczos coefficients is more erratic in the nonchaotic case and less erratic in the chaotic case. This behavior is explored [4, 5] on the Krylov chain as a phenomenon of the Anderson localization. The energy eigenstate $|\omega\rangle$ on the Krylov chain can be decomposed in the Krylov basis as

$$|\omega\rangle = \sum_{n=0}^{n_k-1} \psi_n |\mathcal{O}_n\rangle \quad (3.1)$$

There is a zero frequency state whose solution is given by [4, 5]

$$\frac{\psi_{2n}}{\psi_0} = (-1)^n \prod_{i=1}^n \frac{b_{2i-1}}{b_{2i}}, \quad n = 0, \dots, \frac{n_k-1}{2}. \quad (3.2)$$

The extent of localization can be extracted from this zero frequency state and the disordered coefficients b_n [19]. The localization length is inversely proportional to the variance of the

Lanczos coefficients [5], defined by

$$\sigma^2 := \text{Var}(x_i), \quad x_i = \ln \left| \frac{b_{2i-1}}{b_{2i}} \right|. \quad (3.3)$$

Intuitively, the variance σ^2 measures the magnitude of the erratic behavior of b_n . A smaller variance σ^2 means less erratic behavior of Lanczos coefficients and this gives a larger localization length, so the Krylov chain is more delocalized and this happens when the system is more chaotic. Results in [5] show that the variance σ^2 is indeed smaller in the chaotic case.

The sequence x_i and the variance σ^2 of Lanczos coefficients are computed in the Krylov space $\mathcal{K}_m(\mathcal{L}, \mathcal{O})$ of an initial operator \mathcal{O} . In this paper, we generate samples of random initial operators and do statistics, in order to deal with this dependence on initial operators. It is crucial to analyze the resulting statistics of the sequence x_i and the variance σ^2 , because they characterize the distinction between nonchaotic and chaotic behaviors. In the following, the $\langle \dots \rangle$ means the ensemble average over a sample of initial operators.

To be specific, We focus on the statistics of the more interesting correlation matrix¹ $x_i x_j$, and the resulting distribution f_{σ^2} of the variance σ^2 across a sample. Naively, the resulting statistics of $x_i x_j$ and f_{σ^2} depend on the distributions of the initial operator \mathcal{O} . However, we find that their statistics are the Wishart distribution and the rescaled chi-square distribution respectively, independent of the distribution of initial operators. As the matrix size of the operator increases, they approach the normal distribution, at which time the behavior of f_{σ^2} depends only on whether the system is nonchaotic or chaotic: nearly complete overlapping f_{σ^2} in the nonchaotic case, and two well-separated groups of f_{σ^2} in the chaotic case.

Before showing the explicit results, we qualitatively analyze the statistical properties of Lanczos coefficients in the remaining of this section. We firstly explain the statistics in a purely intuitive manner. Then we explain the statistics using the Wishart distribution [21].

3.1 Intuition on the normal distribution

Firstly we give an intuitive explanation of the reason why the resulting distributions are normal distributions when the size of matrix is large. This is related with the nature of the Krylov algorithm itself and can be understood using the central limit theorem of probability theory.

Intuitively, the matrices involved in the Krylov algorithm depend only on the energy levels and the initial random matrix. This can be seen by the following lemma proved by mathematical induction.

Lemma 1. *Matrix elements $\mathcal{O}_{mn}^{(k)}$ of Krylov basis \mathcal{O}_k in the energy representation can be written as:*

$$\mathcal{O}_{mn}^{(k)} = C_{mn}^{(k)}(b_1, b_2, \dots, b_k; E_{mn}) \mathcal{O}_{mn}^{(0)} \quad (3.4)$$

where $E_{mn} := E_m - E_n$.

¹In statistics, this is the scatter matrix to estimate the covariance matrix of a distribution. Since we are not doing pure mathematics here, we prefer to use the more physical term 'correlation matrix' [20].

Proof. $k = 0, 1$ are clearly true, because

$$\mathcal{O}_{mn}^{(0)} = \mathcal{O}_{mn}^{(0)} \quad (3.5)$$

$$\mathcal{O}_{mn}^{(1)} = \frac{1}{b_1} \mathcal{A}_{mn}^{(1)} = \frac{1}{b_1} (E_{mn} \mathcal{O}_{mn}^{(0)}), b_1 = \|E_{mn} \mathcal{O}_{mn}^{(0)}\| \quad (3.6)$$

Assume that $k - 1, k - 2$ holds, then k also holds, because

$$\mathcal{A}_{mn}^{(k)} = E_{mn} \mathcal{O}_{mn}^{(k-1)} - b_{k-1} \mathcal{O}_{mn}^{(k-2)} \quad (3.7)$$

$$= [E_{mn} C_{mn}^{(k-1)}(b_1, b_2, \dots, b_{k-1}; E_{mn}) - b_{k-1} C_{mn}^{(k-2)}(b_1, b_2, \dots, b_{k-2}; E_{mn})] \mathcal{O}_{mn}^{(0)} \quad (3.8)$$

$$= \tilde{C}_{mn}^{(k)}(b_1, b_2, \dots, b_{k-1}; E_{mn}) \mathcal{O}_{mn}^{(0)} \quad (3.9)$$

and

$$b_k = \|\tilde{C}_{mn}^{(k)}(b_1, b_2, \dots, b_{k-1}; E_{mn}) \mathcal{O}_{mn}^{(0)}\| \quad (3.10)$$

$$\mathcal{O}_{mn}^{(k)} = \frac{1}{b_k} \mathcal{A}_{mn}^{(k)} = C_{mn}^{(k)}(b_1, b_2, \dots, b_k; E_{mn}) \mathcal{O}_{mn}^{(0)}. \quad (3.11)$$

Then by mathematical induction the lemma is proved. \square

From this lemma, we see that all Lanczos coefficients $b_k = b_k(\mathcal{O}_{mn}^{(0)}; E_{mn})$ depend only on the energy levels and the initial random matrix $\mathcal{O}_{mn}^{(0)}$. In practical computation, the energy levels are truncated to \mathcal{N}_{max} and the random matrix $\mathcal{O}_{mn}^{(0)}$ is of size $\mathcal{N}_{max} \times \mathcal{N}_{max}$. If the value of \mathcal{N}_{max} is large, there would be tremendous random numbers. Intuitively, we would expect that the central limit theorem comes into play when we have large-enough random numbers, and the resulting distribution can be estimated by the normal distribution. On the other hand, we can intuitively expect that most information of the system is preserved with a large enough \mathcal{N}_{max} . We know that a chaotic system resembles the behavior of RMT from level statistics. Then a more accurate approximation to the system means more randomness are preserved in this case. So things are random enough such that we can use the central limit theorem to expect the normal distribution.

3.2 Distribution of the average correlation matrix $\langle x_i x_j \rangle$

Now we qualitatively analyze the statistics of the average correlation matrix $\langle x_i x_j \rangle$. Suppose K continuous Lanczos coefficients are selected from the Krylov space of a given initial operator, with K being the algorithmic steps. We shall take the approximation that the sequence $\vec{X} = (x_1, \dots, x_K)$ is a K -component random vector. This is easily understood in the Krylov chain, where by analog with the Anderson localization the Lanczos coefficients are disordered. Without the Krylov chain, it is indeed harder to accept this. Naively looking at the Lanczos algorithm, the Lanczos coefficients seem to be already predetermined by the initial operator, like an initial value problem of ODE. However, we can intuitively get the randomness from Lemma 1. The initial operator is already a random matrix and all Lanczos coefficients are generated from a complicated pipeline of arithmetic of energy levels with the random matrix. And the energy levels themselves are closely related with RMT in the case of chaos. So we can still accept the assumption that \vec{X} is a random vector even without the

help of the Krylov chain. After all, studies in the literature have shown the erratic behavior of Lanczos coefficients in various kinds of systems, and this assumption indeed leads to a successful interpretation of the results in this paper.

After accepting the randomness of x_i , we go one step further by assuming that the K -component random vector $\vec{X} = (x_1, \dots, x_K)$ is from a multivariate normal distribution $N_K(0, \Sigma)$ with zero mean and a covariance matrix Σ of size K . The zero mean is easily understood again in the Krylov chain by the Anderson localization, where the disordered b_n imply that x_i are fluctuating around zero. The property of being normal can be intuitively understood from the analysis in the previous subsection 3.1. Previous numerical results also show this property [4, 6].

With this assumption, the average correlation matrix $\langle x_i x_j \rangle$ is exactly the common estimator used in RMT [20]. For a sample of N random initial operators, we get N random vectors that form a matrix of size $N \times K$

$$X = \left(\vec{X}_1, \vec{X}_2, \dots, \vec{X}_N \right)^T, \quad \vec{X}_i = \left(x_1^{(i)}, x_2^{(i)}, \dots, x_K^{(i)} \right), \quad x_j^{(i)} \in \mathbb{R}, \quad (3.12)$$

where the \vec{X}_i are independent, identically distributed random vectors from $N_K(0, \Sigma)$. Then the sample covariance matrix M is a symmetric square matrix of size K defined as

$$M = X^T X = \sum_{i=1}^N \vec{X}_i^T \vec{X}_i \sim W_K(\Sigma, N), \quad (3.13)$$

which has the probability distribution $W_K(\Sigma, N)$ known as the Wishart distribution. The empirical sample covariance matrix M is the most commonly used estimator for the covariance matrix Σ . If Σ is given, the random vector \vec{X}_i has the distribution

$$N_K(0, \Sigma) \left(\vec{X}_i \right) = \frac{e^{-\frac{1}{2} \text{Tr} \vec{X}_i \Sigma^{-1} \vec{X}_i^T}}{(2\pi)^{K/2} \sqrt{\det \Sigma}} \prod_{j=1}^K dx_j^{(i)} \quad (3.14)$$

the Wishart distribution is defined as

$$P(M) = \frac{1}{2^{NK/2} (\det \Sigma)^{N/2} \Gamma_K \left(\frac{N}{2} \right)} (\det M)^{\frac{N-K-1}{2}} e^{-\frac{1}{2} \text{Tr} \Sigma^{-1} M}, \quad (3.15)$$

where Γ_K is a multivariate generalization of the Gamma function

$$\Gamma_K \left(\frac{N}{2} \right) = \pi^{K(K-1)/4} \prod_{j=1}^K \Gamma \left(\frac{N}{2} - \frac{j-1}{2} \right). \quad (3.16)$$

Note that our average correlation matrix $\langle x_i x_j \rangle$ is exactly the sample covariance matrix M , because $\langle x_i x_j \rangle = M_{ij}/N$. So it can indeed capture the statistics behind the ensemble average and we can use properties of the Wishart distribution to understand its behavior. The Wishart distribution can be viewed as a multi-variate generalization of the chi-squared distribution as follows: if $K = \Sigma = 1$, it reduces to the chi-squared distribution with N degrees of freedom. However, this is exactly the case in this paper. The distributions of initial operators we used (2.8)-(2.10) are univariate, whose Σ is the identity matrix. Then it

is naturally to expect that the resulting K -component random vector \vec{X} is also univariate. So we can refine the previous assumption by expecting that \vec{X} is from a univariate normal distribution $N(0, \sigma_x)$. In this way, the Wishart distribution satisfied by $\langle x_i x_j \rangle$ reduces to the chi-square distribution of $\langle x_i^2 \rangle$. In Figure 1a, we show the histogram of $\langle x_i^2 \rangle$ for the case of GUE when the system is chaotic with $\mathcal{N}_{max} = 15$. It is indeed the chi-square distribution. As the size of matrix increases, the distribution would become normal by the central limit theorem. In Figure 1b, the corresponding histogram of $\langle x_i x_j \rangle$ with $\mathcal{N}_{max} = 50$ is plotted and it is indeed the normal distribution. Similarly properties are there when the system is nonchaotic.

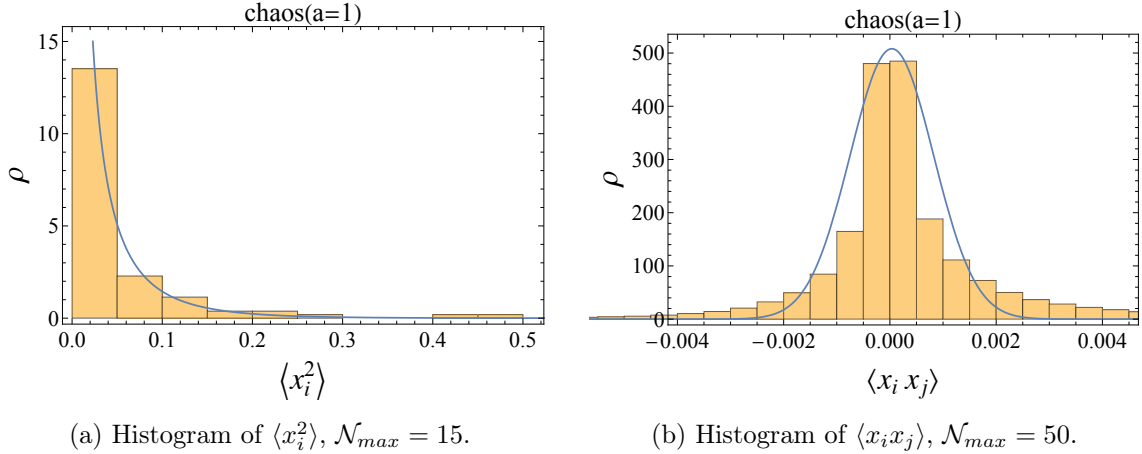


Figure 1: Distribution of $\langle x_i x_j \rangle$ in the chaotic case.

3.3 Distribution f_{σ^2} of the variance σ^2

Now we have a qualitative understanding of the statistics of the average correlation matrix $\langle x_i x_j \rangle$ from the aspect of the Wishart distribution. What about the statistics of the resulting distribution f_{σ^2} of the variance? We expect it to follow the same distribution as the average correlation matrix.

For convenience, suppose the variance $\sigma_{\mathcal{O}}^2$ is computed from $K = 2p$ Lanczos coefficients for a given initial operator \mathcal{O} . By definition (3.3), we have

$$\sigma_{\mathcal{O}}^2 = \frac{1}{p} \sum_{i=1}^p x_i^2 - \frac{1}{p^2} \left(\sum_{i=1}^p x_i \right)^2 = \left(\frac{1}{p} - \frac{1}{p^2} \right) \sum_{i=1}^p x_i^2 - \frac{1}{p^2} \sum_{i \neq j} x_i x_j. \quad (3.17)$$

Qualitatively, we can expect that the second term with $i \neq j$ can be neglected compared with the first term. This is true when the set size K is large. In the detailed computation of this paper, this condition is satisfied and the second term is smaller than the first term by at least one order of magnitude. So we obtain qualitatively

$$\sigma_{\mathcal{O}}^2 \sim \left(\frac{1}{p} - \frac{1}{p^2} \right) \sum_{i=1}^p x_i^2. \quad (3.18)$$

In the previous subsection 3.2, we have discussed the physics that x_i are independent random variables from a univariate normal distribution $N(0, \sigma_x)$. If the standard deviation σ_x is known, we can scale x_i by an overall factor to make its standard deviation being 1. In this way, the resulting distribution f_{σ^2} (3.18) is proportional to the chi-square distribution by an overall factor, called the rescaled chi-square distribution here. When \mathcal{N}_{max} increases, it would approach the normal distribution.

Numerical results indeed support this expectation. In Figure 2, we show the histogram of the variance σ^2 for the case of GOE when the system is chaotic. When $\mathcal{N}_{max} = 5$, the histogram clearly satisfies the rescaled chi-square distribution with the curve being the fitted distribution. As it increases to $\mathcal{N}_{max} = 100$, the histogram approaches the normal distribution and the curve are the fitted normal distribution. Similar properties are there for the other ensembles and for the nonchaotic case, as discussed in Section 4 and Appendix C.

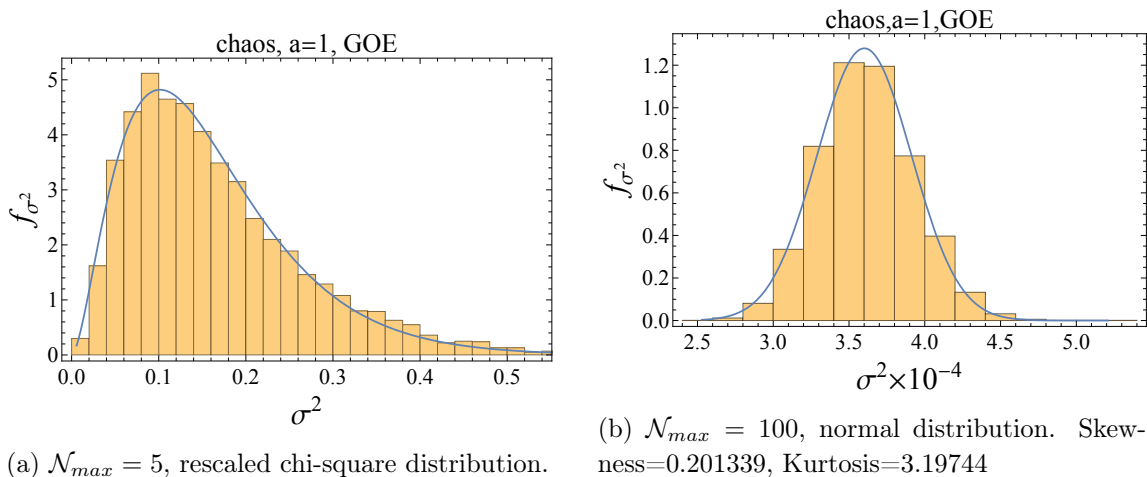


Figure 2: Chi-square distribution of f_{σ^2} in the chaotic case for GOE.

From this section's analysis, we see that the amount of random numbers is determined by \mathcal{N}_{max} , K and the sample size N of initial operators. If they are large enough, we would expect the resulting distribution to be normal. In the following computation, we use the choice $\mathcal{N}_{max} = 100$ and $K = 500$ in consistent with [13], and we average over $N = 5000$ initial operators. This number turns out to be large enough and the resulting distribution function f_{σ^2} is the normal distribution.

4 Model and Results

For concrete, we study the Sinai billiard which is a typical two-dimensional system of chaos. The Hamiltonian is defined by

$$H = p_x^2 + p_y^2 + V(x, y) \quad (4.1)$$

with the potential

$$V(x, y) = \begin{cases} 0 & (x, y) \in \Omega \\ \infty & \text{else} \end{cases}. \quad (4.2)$$

The region Ω is obtained by cutting out a circle of radius l from an equilateral triangle of side length L , as shown in Figure 3. The system is integrable when $l = 0$ and chaotic when $0 < l < L$. For convenient, the area of Ω is kept at 1 and the parameter $a \equiv l/L$ is introduced, whose value determines the degree of chaos for the system.

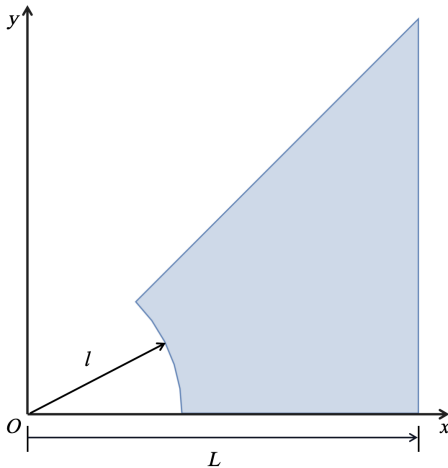


Figure 3: The region Ω of the potential (4.2) of the billiard. Dirichlet conditions are imposed on the boundaries.

For practical computation in the energy representation, we need to set the value of \mathcal{N}_{max} to truncate the number of energy levels. It is adequate to take a value as long as the resulting distributions of $\langle x_i x_j \rangle$ and f_{σ^2} are normal. When this happens, there are enough randomness in the statistics so that $\langle x_i x_j \rangle$ and f_{σ^2} can distinguish the chaotic and the nonchaotic behaviors. Empirically, $\mathcal{N}_{max} = 50$ is enough here. For the average correlation matrix $\langle x_i x_j \rangle$, we use $\mathcal{N}_{max} = 50$ for the purpose of numerical efficiency. For the distribution f_{σ^2} of the variance, we use $\mathcal{N}_{max} = 100$ to keep accordance with [13]. Then we pick a random matrix $\mathcal{M}_{\mathcal{O}}$ of size $\mathcal{N}_{max} \times \mathcal{N}_{max}$ from the probability distributions (2.8)-(2.10) for the initial random operator \mathcal{O} . After that, we compute the Lanczos coefficient $\{b_n\}$ of $\mathcal{K}_m(\mathcal{L}, \mathcal{M}_{\mathcal{O}})$ by the algorithm in Section 2. To calculate the variance σ^2 of Lanczos coefficients, we choose the set size to be $K = 5\mathcal{N}_{max}$, in consistent with [13]. Finally, we repeat this process $N = 5000$ times to get the resulting distribution of $\langle x_i x_j \rangle$ and f_{σ^2} .

In Figure 4, an example of Lanczos coefficients b_n for the case of GUE is shown. There is a clear difference between the chaotic and the nonchaotic case, which can be explored further by the average correlation matrix $\langle x_i x_j \rangle$. The set of coefficients $\{b_n\}$ between the two red lines, $5\mathcal{N}_{max} \leq n \leq 10\mathcal{N}_{max}$, is selected to compute the variance σ^2 . Note that this selection of the set does not qualitatively affect the result of this paper. The effect of selecting the set of $\{b_n\}$ from different algorithm step sizes is discussed in the appendix B.

In Figure 5, the average correlation matrix $\langle x_i x_j \rangle$ is shown for the case of GUE. With $\mathcal{N}_{max} = 50$, its histogram approaches the normal distribution as shown in Figure 1b so that there is enough randomness in the statistics. There is a clear distinction in the pattern between the chaotic and the nonchaotic case. In the nonchaotic case, there are heavy cross-like structures with large matrix values. But in the chaotic case, these heavy cross-like structure disappears (or fades away) and matrix values are more uniformly or smoothly distributed.

In Figure 6, the variances σ^2 are shown for the samples of different distributions (GOE, GUE, URE, UIM and UCP) of initial operators, where m labels the sample. Note that only the first 1000 out of the total 5000 samples are shown for the purpose of visual clearness, and the remaining samples have similar behaviors. For GOE and GUE, they overlap completely in the nonchaotic case in Figure 6b, and separate from each other in the chaotic case in Figure 6a. Similarly for the uniform distributions, they mix together in the nonchaotic case in Figure 6d, and split into two separated groups in the chaotic case in Figure 6c, with URE and UIM being one group and UCP being the other.

In Figure 7, the histogram of all the sampled σ^2 is shown and the resulting probability distribution resembles the normal distribution. For the Gaussian ensembles, we can see clearly that they are overlapped in the nonchaotic case in Figure 7b and separated in the chaotic case in Figure 7a. For the uniform distributions, they are overlapped in the nonchaotic case in Figure 7d. In the chaotic case in Figure 7c, URE and UIM are still together, but they are separated from UCP.

Figures 6 and 7 straightforwardly show that the resulting distributions f_{σ^2} can distinguish the chaotic and the nonchaotic behaviors. Their axis values indicate that they can be compared together in one plot. So we fit² their histogram to the normal distribution and find the average value $\langle \sigma^2 \rangle$ and the standard deviation, which can characterize the resulting distribution f_{σ^2} . Then the resulting distribution f_{σ^2} can be shown in one plot where the point is this average value and the error bar is the standard deviation. In Figure 8, the resulting distributions f_{σ^2} are shown for all different distributions (GOE, GUE, URE, UIM and UCP) of initial operators, as the system varies from nonchaotic $a = 0$ to chaotic $a = 1$. When the system is nonchaotic, the data points of all distributions overlap together within the range of error bars. As the system becomes chaotic, different distributions start to separate approximately at $a = 0.1$ and the distance of separation is roughly fixed after $a = 0.15$. Note that the axis is logarithmic, so the separation is very large. We see that they split into two groups well-separated: one group is of GOE, URE and UIM, the other group is GUE and UCP.

5 Discussion

To begin, the average correlation matrix $\langle x_i x_j \rangle$ has different patterns between the nonchaotic and the chaotic case, as shown in Figure 5. From the aspect of RMT, the average correlation matrix $\langle x_i x_j \rangle$ is the common estimator of the statistics. So different patterns qualitatively tell us that the statistics of $\langle x_i x_j \rangle$ can distinguish between the nonchaotic and

²The details of this data fitting is shown in the Appendix A.

the chaotic case. On the other hand, x_i characterizes the disorderedness of Lanczos coefficients from the aspect of the Krylov chain. So $\langle x_i x_j \rangle$ quantitatively captures the erratic behavior and the correlation of Lanczos coefficients. In the nonchaotic case of Figure 5b, the large matrix values indicate more erratic behavior of Lanczos coefficients and more localization on the Krylov chain. So it provides another view for the connection between chaos and Anderson localization and is consistent with results of [5, 18].

The repetition of the heavy cross-like structure in Figure 5b is also a very interesting phenomenon. It might come from some abstract periodic boundary conditions of the Krylov chain. Or it might be connected to the phenomenon of two-electron correlations of Anderson localization on the Krylov chain [14]. In Figure 9, we plot the average correlation matrix of the wave function $\langle \ln |\psi_{2m} \psi_{2n}| \rangle$ for the zero frequency state of the Krylov chain. There are also heavy cross-like structures for the nonchaotic case in Figure 9b. These cross-like structures locally look like the cross-like structure of the two-electron correlations of Anderson localization in disordered mesoscopic ring [14]. And the cross-like structure of $\ln |\psi_{2m} \psi_{2n}|$ disappears in the chaotic case in Figure 9a. The physics of this structure remains an open problem at this stage.

Then, we emphasize that these overlapping-separating behaviors do not depend on the choice of algorithm step-sizes of coefficients $\{b_n\}$. In appendix B, we choose the step-sizes $10\mathcal{N}_{max} \leq n \leq 15\mathcal{N}_{max}$ from the Krylov space in Figure 4. We still get the resulting normal distributions and the overlapping-splitting behaviors. Note that the detailed values of the average and the standard deviation will change, it is the overlapping-separating behavior that does not change. It remains an open problem to quantitatively prove this independence on different choices of algorithm step-sizes.

In addition, we emphasize the importance of the resulting distribution being the normal distribution. We repeat the computation for $\mathcal{N}_{max} = 5$ in Appendix C, where the resulting distribution f_{σ^2} is not normal and there is no separation of f_{σ^2} in the chaotic case. This suggests that the resulting distributions being normal is essential for their separation behavior in the chaotic case.

Qualitatively we can understand this by the central limit theorem as discussed in Section 3. The resulting distribution being normal means that we have enough randomness in the sample, so that the statistics is reliable and robust. Empirically, a choice of $\mathcal{N}_{max} = 50$ is already adequate to get the normal distribution. It remains an open problem to quantitatively understand the connection between being normal distributions and the separation behavior of f_{σ^2} .

After that, we discuss the resulting two groups of separation. The GOE, URE and UIM are in one group. We can view GOE, URE and UIM as essentially composed of only real numbers, because the UIM is just real numbers multiplied by the overall factor-the imaginary i . The other group is GUE and UCP, which are essentially composed of complex numbers with both real and imaginary parts. So one group is essentially related with one-dimensional random numbers and the other group is related with two-dimensional random numbers. This distinction between real and complex numbers may be related to the nature of the integrability-breaking-term, or to the symmetry of the model [22]. This remains to be one of the open problems.

Finally, we explain a connection (or equivalence) between the average over initial operators and the RMT Hamiltonians. For the chaotic case, a similar behavior-of-separation is obtained related with RMT [6]. For a spin system [6] under chaotic dynamics, the Hamiltonian is sampled from RMT ensembles while the initial operator is fixed. For Hamiltonians from GUE and GOE, a separation is obtained in the late-time saturation of the Krylov complexity. Qualitatively, the behavior of late-time saturation of K-complexity are consistent with the behavior of variances σ^2 of the Lanczos coefficients [5]. So it might be possible that the ensemble average of the variance σ^2 over RMT Hamiltonian are also separating in [6], although it is not computed there. If this indeed happen, the separation behavior of the resulting distributions f_{σ^2} and of the late-time saturation of the Krylov complexity can be viewed as 'dual' to each other for chaotic systems.

Another sign for this 'duality' also appears in the study of the spin chain [4]. There the randomness is introduced by the random transverse field from a uniform distribution. So it is equivalent to a RMT Hamiltonian. There the statistics is focused on the parameters of the linear extrapolation formula of Lanczos coefficients. These fitted parameters also follow the normal distribution, similar to the resulting distribution f_{σ^2} , although they are completely different quantities. This suggests that the statistics would be normal as long as there is enough randomness, whether it is due to random initial operators or RMT Hamiltonians.

Qualitatively, this 'duality' can be understood as follows: in one side, the Hamiltonian are random and the initial operator is fixed, and in the other side, the Hamiltonian is fixed and the initial operators are random. They are 'equivalent' when taking the statistics, at least for chaotic systems. From the proof (3.10) of the lemma in Section 3, we see that the Lanczos coefficients and the Krylov basis depend only on the initial operators and energy levels. Both the random energy levels and random initial operators can give random Lanczos coefficients, so intuitively, these statistics can be viewed as dual or equivalent. It remains an open problem to quantitatively prove this duality. In [5], the Lanczos coefficients are rewritten in terms of the Hankel determinants of level spacings, which might be helpful in this direction.

In conclusion, we find two statistical quantities that have distinct behaviors as the Sinai billiard system changes from nonchaotic to chaotic, i.e., the average correlation matrix $\langle x_i x_j \rangle$ and the resulting distribution f_{σ^2} of the variance of Lanczos coefficients. The statistics of these two quantities are the Wishart distribution and the rescaled chi-square distribution respectively, independent of distributions of initial operators. When the chi-square distribution approaches the normal distribution, the resulting distributions f_{σ^2} can distinguish the nonchaotic and the chaotic regime: they are overlapped in the nonchaotic case and they split into two groups in the chaotic case. The average correlation matrix $\langle x_i x_j \rangle$ also exhibits different patterns in the nonchaotic and the chaotic regime: there are heavy cross-like structures in the nonchaotic case. These results provide a dual view on results in the literature and reveal a deeper connection among Lanczos coefficients, RMT and the Anderson localization.

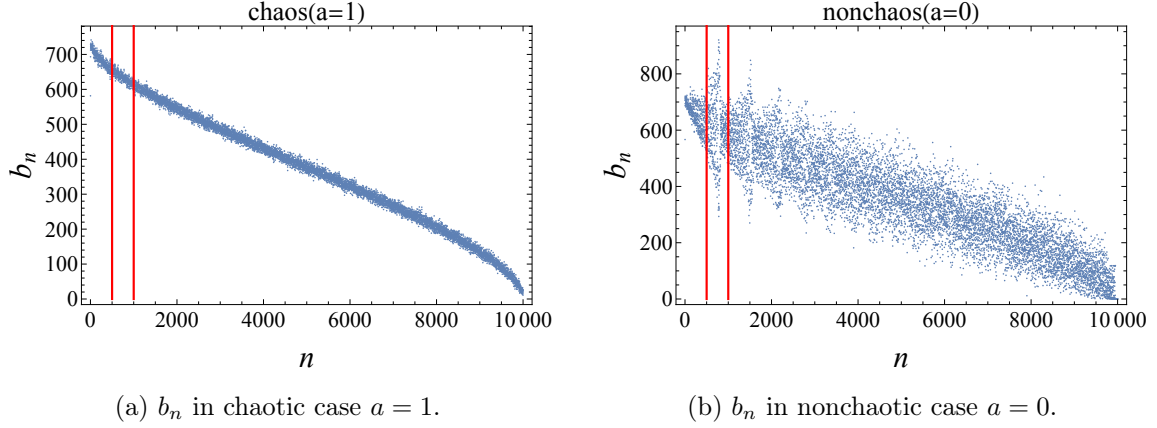


Figure 4: The Lanczos coefficients $\{b_n\}$ for an initial operator selected from GUE. The sets of coefficients between the two red lines ($500 \leq n \leq 1000$) are used to calculate the variance σ^2 (3.3).

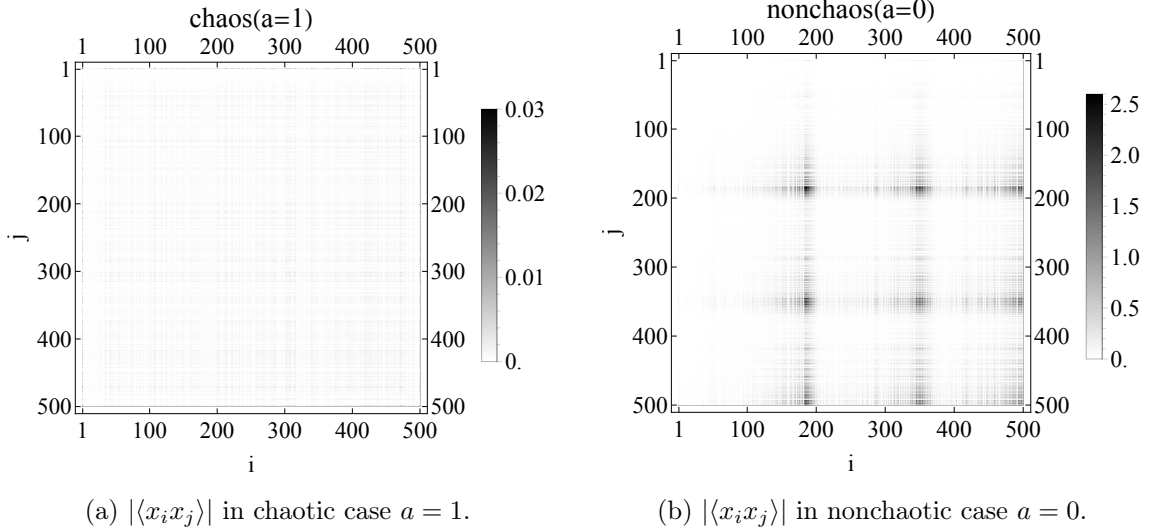


Figure 5: Patterns of $|\langle x_i x_j \rangle|$ with $\mathcal{N}_{max} = 50$

Acknowledgments

Wei Fan is supported in part by the National Natural Science Foundation of China under Grant No. 12105121.

A Check the normal distribution of σ^2 for $\mathcal{N}_{max} = 100$

Here we show the data fitting of the histogram in Figure 7 to the normal distribution. For GOE and GUE, the fitted distribution is shown in Figure 10. For uniform distributions, the fitted distribution is shown in Figure 11. The average value and the standard deviation are listed in Table 1, where we compare the values obtained from the sampled data and from the fitted normal distribution.

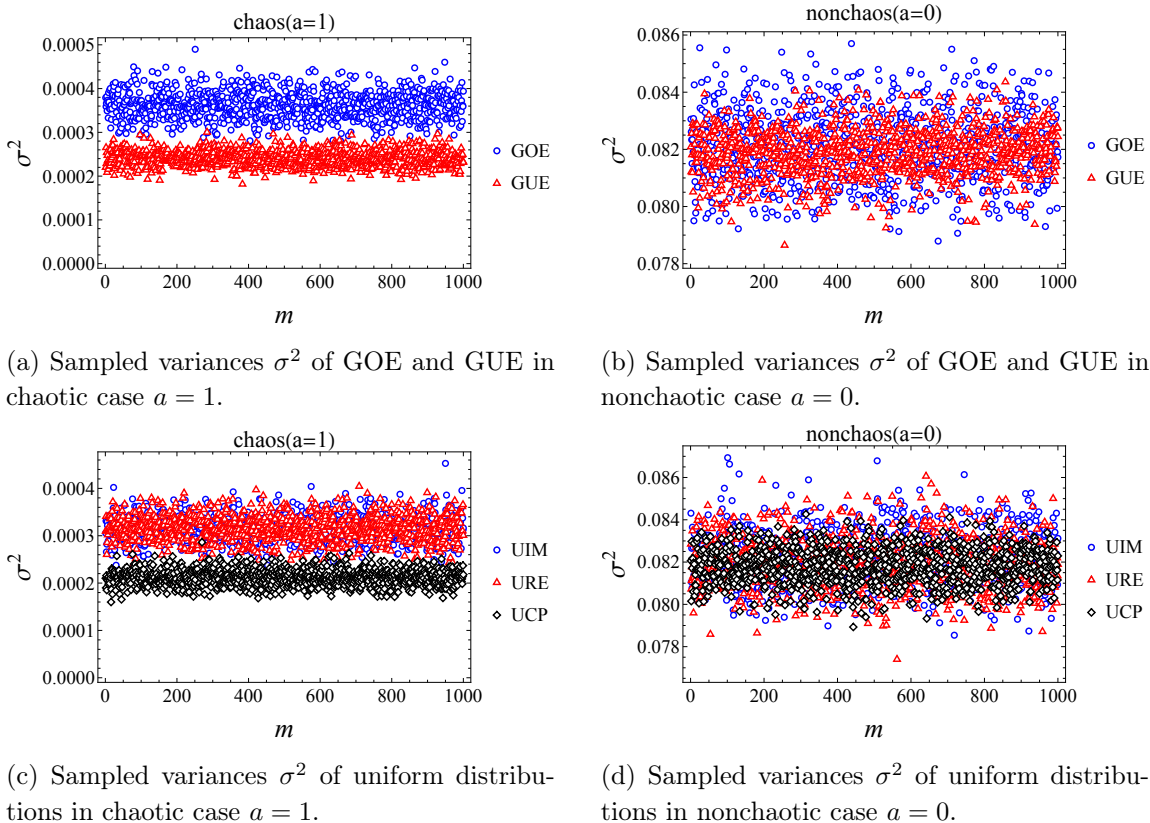


Figure 6: Samples of variances σ^2 for GOE, GUE, URE, UIM and UCP. The horizontal axis represents the m th sampling. The chaotic $a = 1$ and nonchaotic case $a = 0$ have different behaviors.

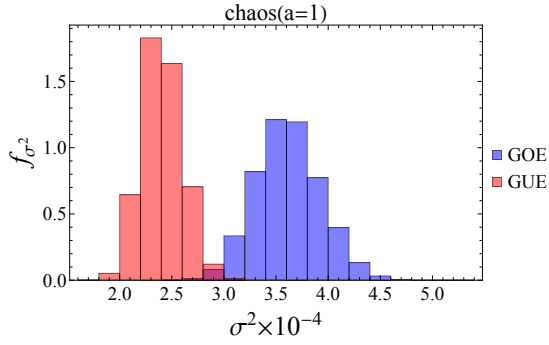
B Different choice of algorithm step sizes for b_n

For the overlapping-separating behavior, here we show its independence on the sets of coefficients used in computing σ^2 . Now we choose the Lanczos coefficients $\{b_n\}$ from step-sizes $10\mathcal{N}_{max} \leq n \leq 15\mathcal{N}_{max}$ of Figure 4.

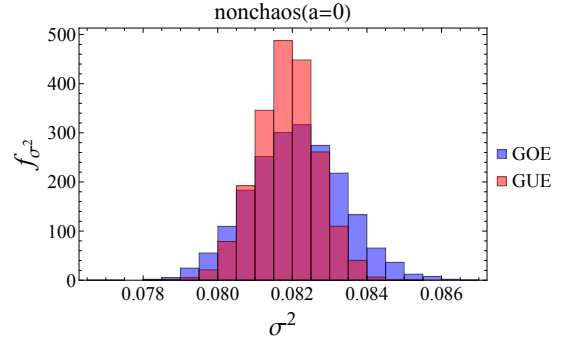
Firstly, we compute the variance σ^2 (3.3), where the first 1000 samples are shown in Figure 12. We see that they mix together in the nonchaotic case and separate from each other in the chaotic case.

Then, the histogram of all 5000 samples are shown in Figure 13. Obviously they still resemble normal distributions and are overlapped in the nonchaotic case and well-separated in the chaotic case.

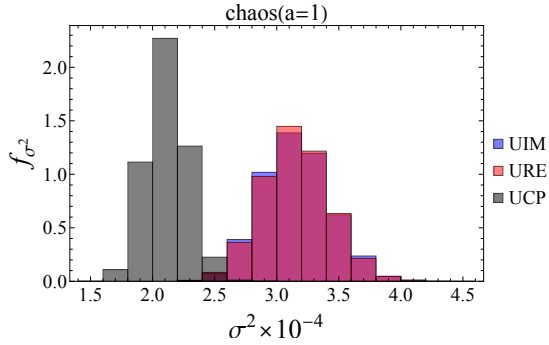
Finally, the fitted normal distributions are shown in Figure 14 and 15. So we still get the resulting normal distributions and the overlapping-splitting behaviors, although the detailed values of the average and the standard deviation change.



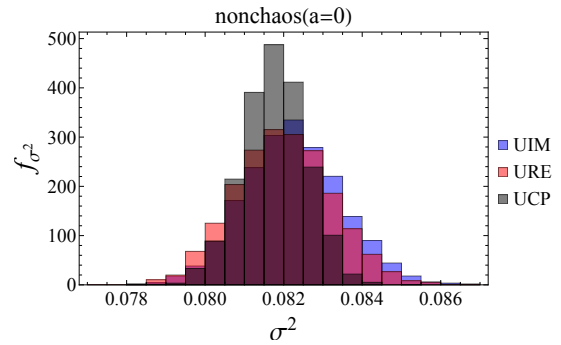
(a) Histogram of σ^2 of GOE and GUE in the chaotic case $a = 1$.



(b) Histogram of σ^2 of GOE and GUE in the nonchaotic case $a = 0$.



(c) Histogram of σ^2 of uniform distributions in the chaotic case $a = 1$.



(d) Histogram of σ^2 of uniform distributions in the nonchaotic case $a = 0$.

Figure 7: The histogram of variances σ^2 after sampling the initial operator 5000 times from GOE, GUE, URE, UIM and UCP. The property of being normal and the overlapping-separating behavior are obvious.

C Check the chi-square distribution of σ^2 for $\mathcal{N}_{max} = 5$

Here we study the case of $\mathcal{N}_{max} = 5$. Then the sets of coefficients b_n are chosen from step-sizes $1 < n < 15$. We repeat the computation and show that there is neither normal distributions nor separating behaviors.

The histogram of all 5000 samples are shown in Figure 16. Obviously they are not normal distributions and are not separated in the chaotic case. So the normal distribution is necessary for the overlapping-separating behavior.

We fit the histogram to the rescaled chi-square distribution, the results are shown in Figure 17 for the Gaussian ensembles and in Figure 18 for the uniform distributions,. We see that the rescaled chi-square distribution indeed captures the resulting distribution f_{σ^2} , so it verifies our analysis in Section 3.3.

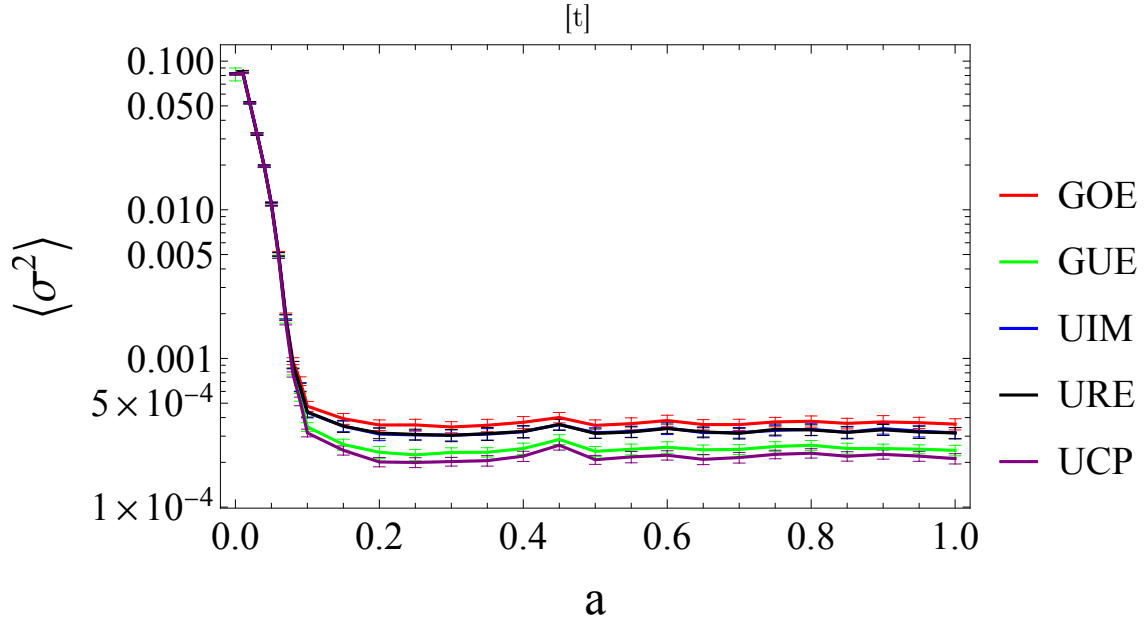
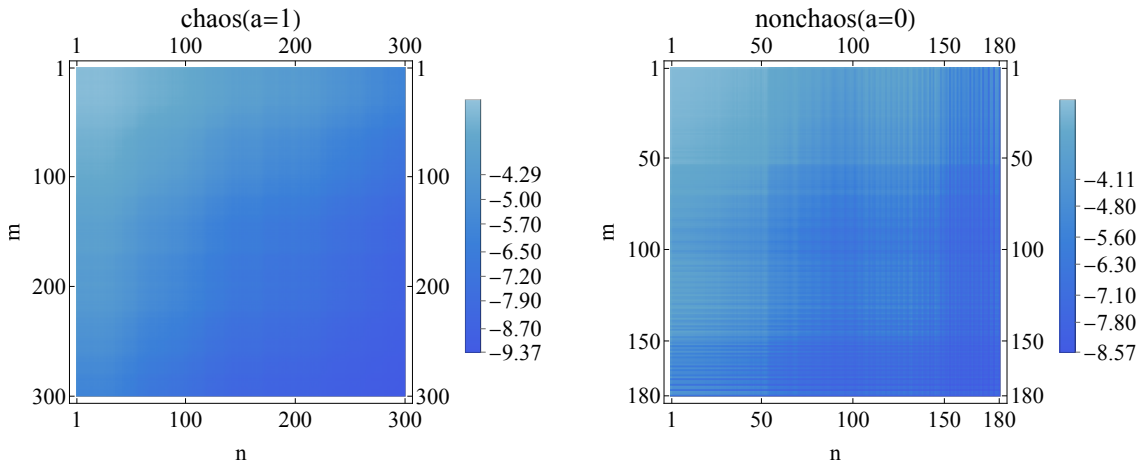


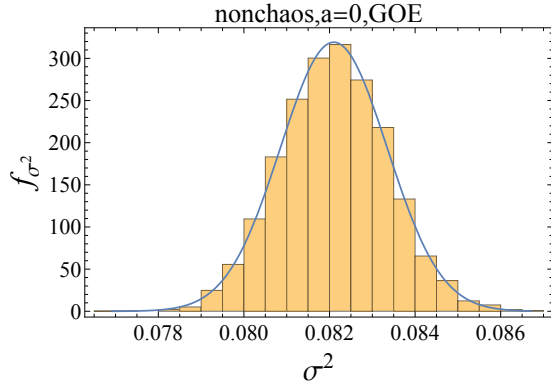
Figure 8: The logarithm plot for the average $\langle \sigma^2 \rangle$ of the resulting normal distribution f_{σ^2} , for all different distributions of initial operators. The error bar is the standard deviation. The system dynamics changes from nonchaotic to chaotic, as a varies from 0 to 1.



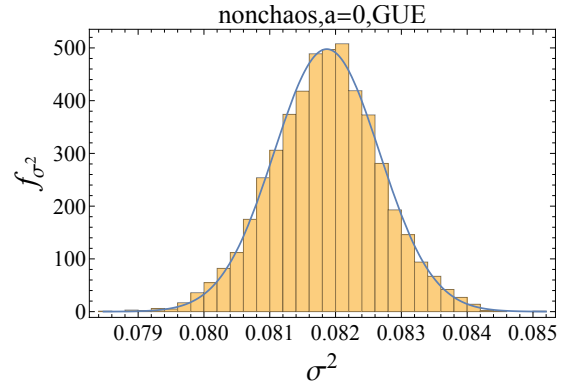
(a) $\langle \ln |\psi_{2m} \psi_{2n}| \rangle$ in chaotic case $a = 1$.

(b) $\langle \ln |\psi_{2m} \psi_{2n}| \rangle$ in nonchaotic case $a = 0$.

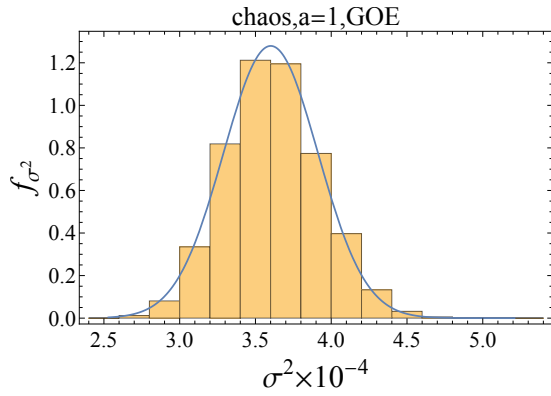
Figure 9: Patterns of $\langle \ln |\psi_{2m} \psi_{2n}| \rangle$ with $\mathcal{N}_{max} = 50$



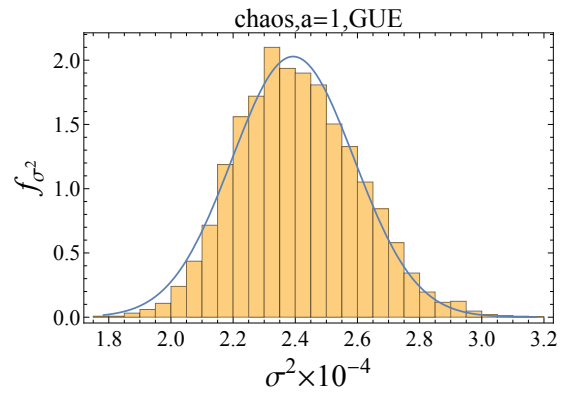
(a) Nonchaotic case $a = 0$ of GOE. Skewness=0.0592927, Kurtosis=3.02995



(b) Nonchaotic case $a = 0$ of GUE. Skewness=-0.06833, Kurtosis=3.13681

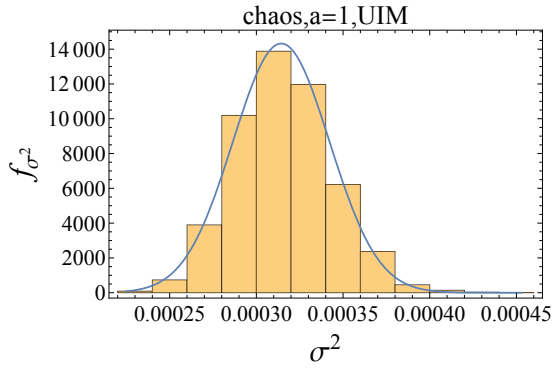


(c) Chaotic case $a = 1$ of GOE. Skewness=0.201339, Kurtosis=3.19744

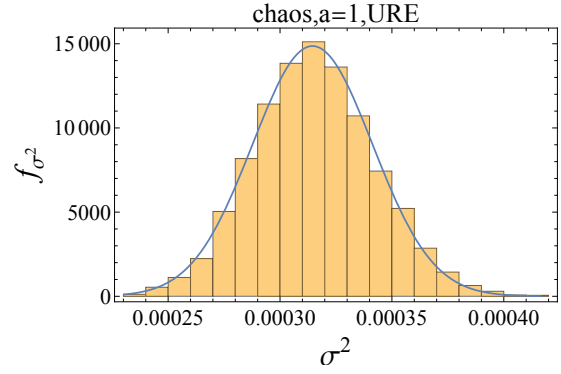


(d) Chaotic case $a = 1$ of GUE. Skewness=0.247936, Kurtosis=2.98557

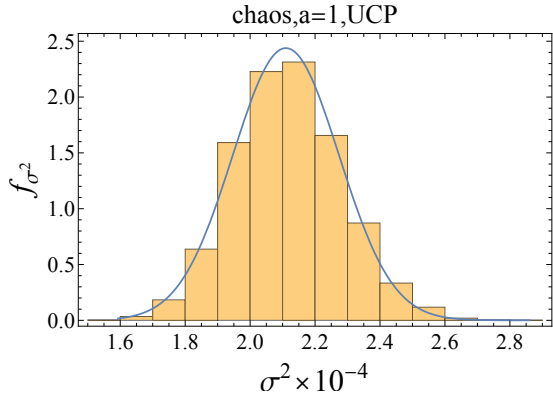
Figure 10: Fitted normal distribution for GOE and GUE, $\mathcal{N}_{max} = 100$.



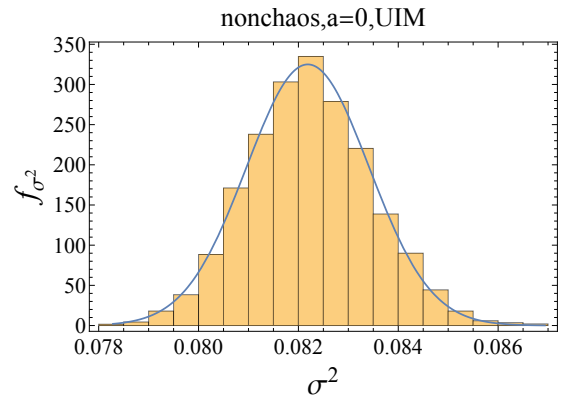
(a) Chaotic case $a = 1$ of UIM. Skewness=0.225317, Kurtosis=3.18781.



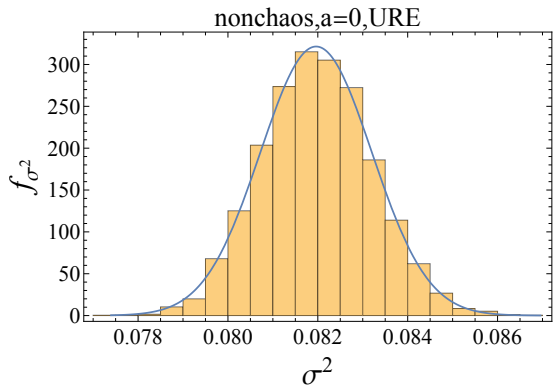
(b) Chaotic case $a = 1$ of URE. Skewness=0.131034, Kurtosis=3.00302.



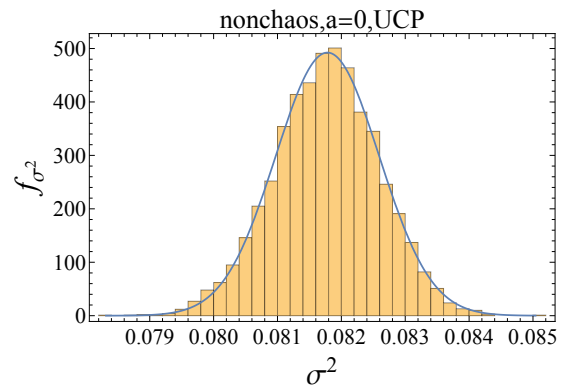
(c) Chaotic case $a = 1$ of UCP. Skewness=0.167094, Kurtosis=3.06099.



(d) Nonchaotic case $a = 0$ of UIM. Skewness=0.1411, Kurtosis=3.08718.



(e) Nonchaotic case $a = 0$ of URE. Skewness=0.0823458, Kurtosis=2.97123.

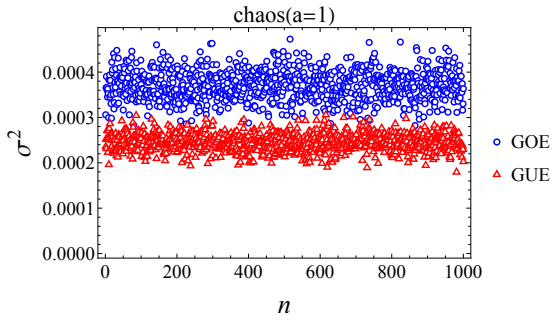


(f) Nonchaotic case $a = 0$ of UCP. Skewness=-0.0801398, Kurtosis=3.04548.

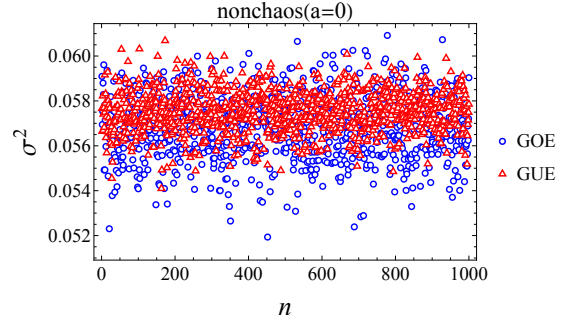
Figure 11: Fitted normal distribution for uniform distributions, $\mathcal{N}_{max} = 100$.

		$\mathcal{N}_{max} = 100$		
		μ_0	σ_0	
nonchaos	GOE	Fit	0.08205	0.00125033
		Data	0.0821079	0.00124627
	GUE	Fit	0.0818423	0.000799776
		Data	0.0818522	0.000818971
	URE	Fit	0.0819622	0.0012411
		Data	0.0819846	0.0012243
	UIM	Fit	0.0821883	0.00122778
		Data	0.0822335	0.00124233
	UCP	Fit	0.0817821	0.000810266
		Data	0.0817644	0.000816963
chaos	GOE	Fit	0.000360084	0.0000311866
		Data	0.000361536	0.0000312431
	GUE	Fit	0.000239301	0.0000196699
		Data	0.00024081	0.0000194523
	URE	Fit	0.000314526	0.0000268396
		Data	0.000315565	0.0000270371
	UIM	Fit	0.000314332	0.0000278555
		Data	0.000315618	0.0000277744
	UCP	Fit	2.11016	0.163631
		Data	2.11775	0.164331

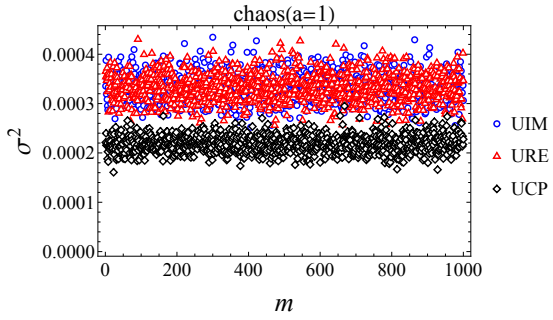
Table 1: Average μ_0 and standard deviation σ_0 for the data fitting, $\mathcal{N}_{max} = 100$. 'Data' means the values computed from the sampled data. 'Fit' means the values of the fitted normal distribution.



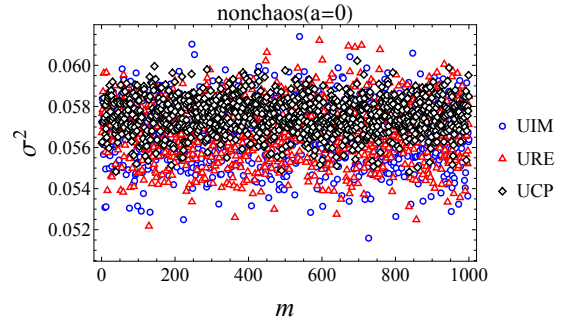
(a) Sampled variances σ^2 of GOE and GUE in chaotic case $a = 1$.



(b) Sampled variances σ^2 of GOE and GUE in nonchaotic case $a = 0$.

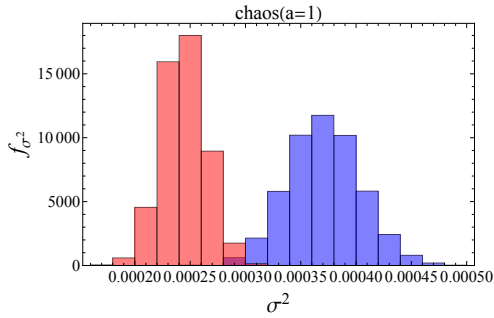


(c) Sampled variances σ^2 of uniform distributions in chaotic case $a = 1$.

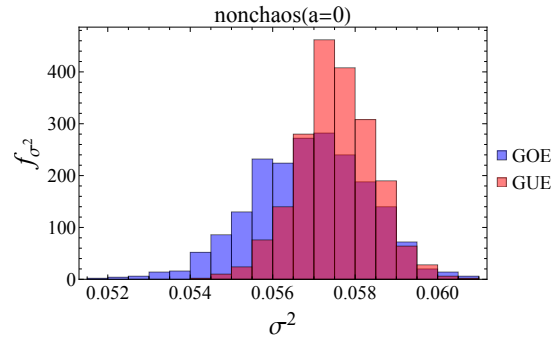


(d) Sampled variances σ^2 of uniform distributions in nonchaotic case $a = 0$.

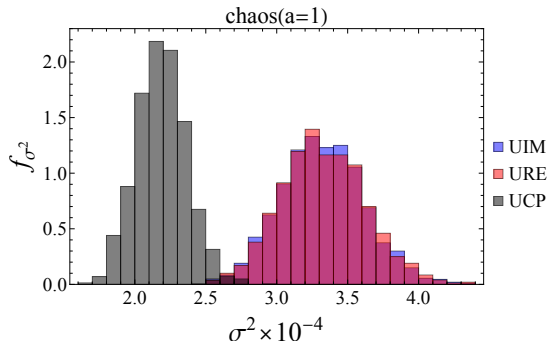
Figure 12: The first 1000 samples of variances σ^2 for GOE, GUE, URE, UIM and UCP. Here the Lanczos coefficients $\{b_n\}$ from step-sizes $1000 \leq n \leq 1500$ are used.



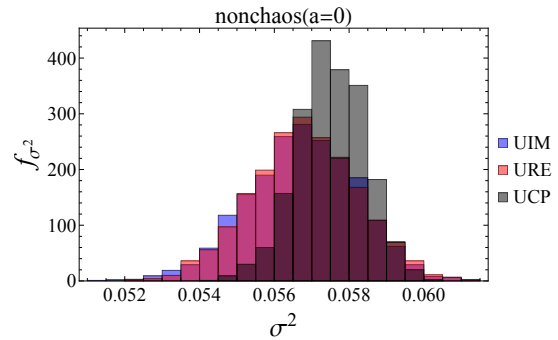
(a) Histogram of σ^2 of GOE and GUE in the chaotic case $a = 1$.



(b) Histogram of σ^2 of GOE and GUE in the nonchaotic case $a = 0$.

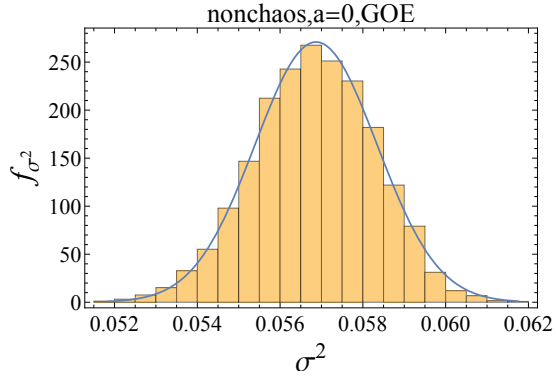


(c) Histogram of σ^2 of uniform distributions in the chaotic case $a = 1$.

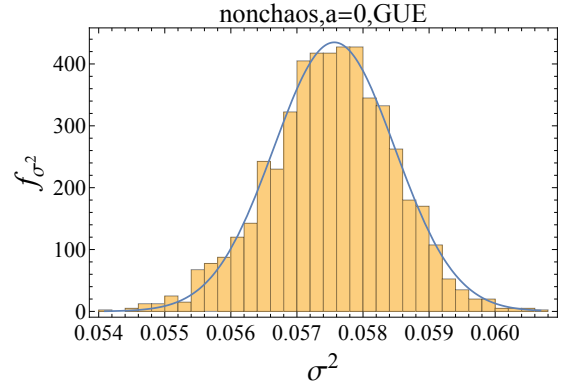


(d) Histogram of σ^2 of uniform distributions in the nonchaotic case $a = 0$.

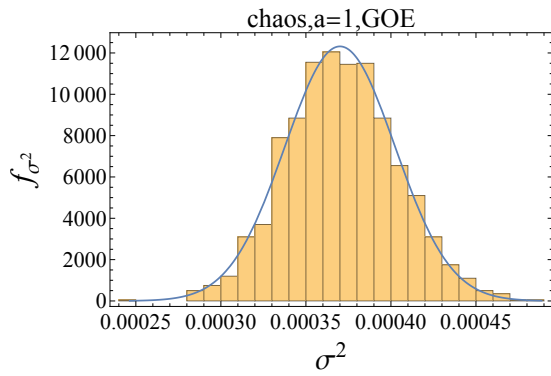
Figure 13: The histogram of variances σ^2 after sampling the initial operator 5000 times from GOE, GUE, URE, UIM and UCP. The Lanczos coefficients $\{b_n\}$ from step-sizes $1000 \leq n \leq 1500$ are used. They are overlapped in the nonchaotic case and well-separated in the chaotic case.



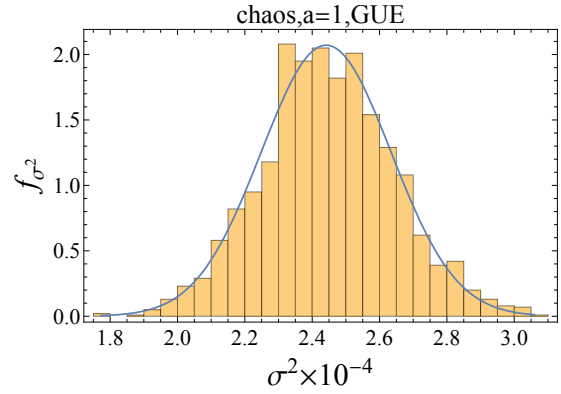
(a) Nonchaotic case $a = 0$ of GOE. Skewness= -0.113535 , Kurtosis= 2.94238 .



(b) Nonchaotic case $a = 0$ of GUE. Skewness= -0.156533 , Kurtosis= 3.16475 .

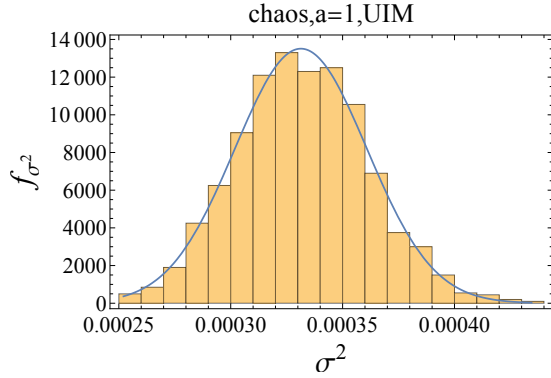


(c) Chaotic case $a = 1$ of GOE. Skewness= 0.107514 , Kurtosis= 3.01354 .

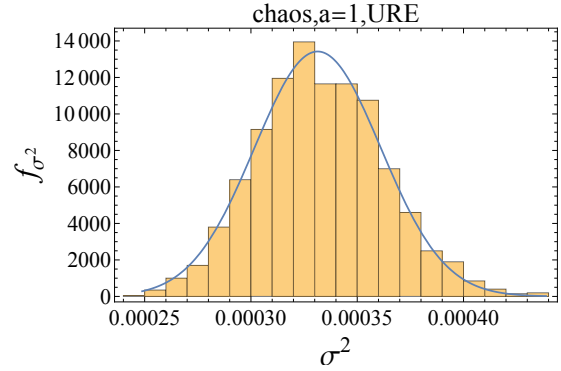


(d) Chaotic case $a = 1$ of GUE. Skewness= 0.0881284 , Kurtosis= 3.06162 .

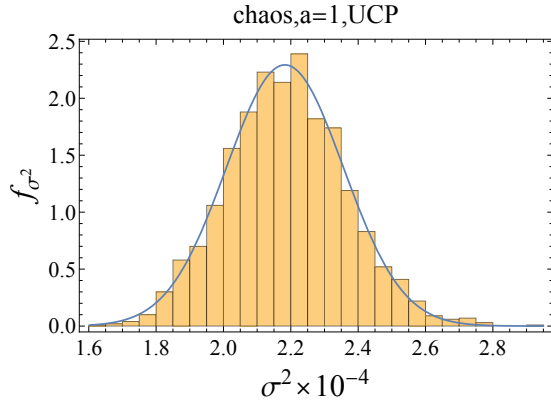
Figure 14: Fitted normal distribution for GOE and GUE, $\mathcal{N}_{max} = 100$. The Lanczos coefficients $\{b_n\}$ from step-sizes $1000 \leq n \leq 1500$ are used.



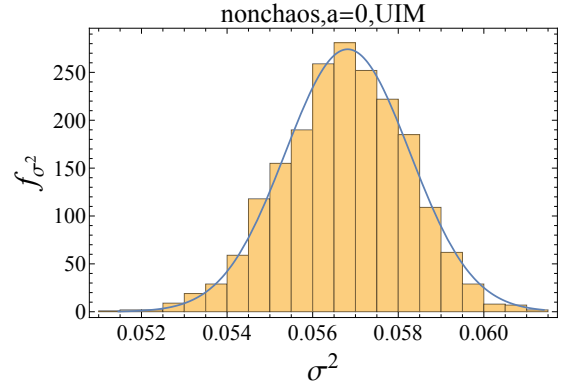
(a) Chaotic case $a = 1$ of UIM. Skewness=0.160477, Kurtosis=3.02122.



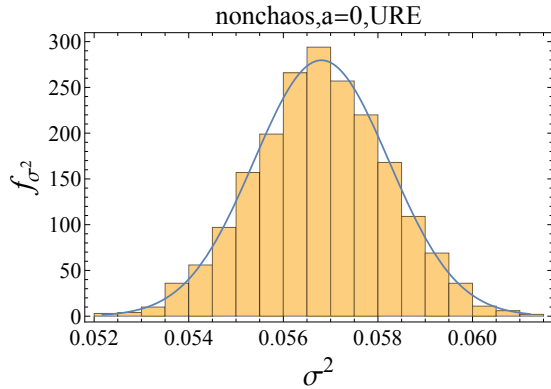
(b) Chaotic case $a = 1$ of URE. Skewness=0.200908, Kurtosis=3.02255.



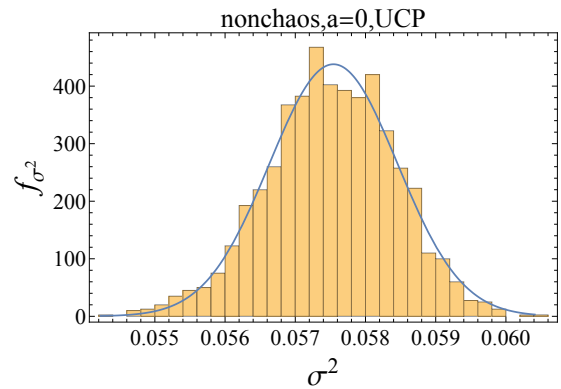
(c) Chaotic case $a = 1$ of UCP. Skewness=0.181879, Kurtosis=3.18625.



(d) Nonchaotic case $a = 0$ of UIM. Skewness=-0.165951, Kurtosis=3.02278.

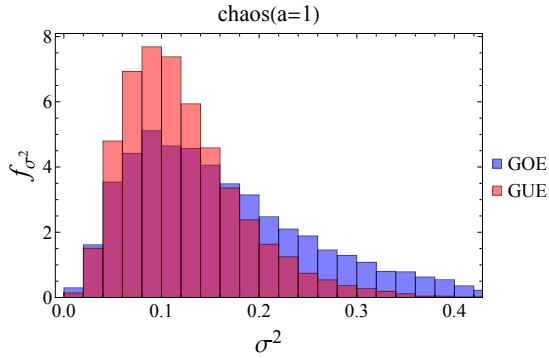


(e) Nonchaotic case $a = 0$ of URE. Skewness=-0.0222373, Kurtosis=2.87503.

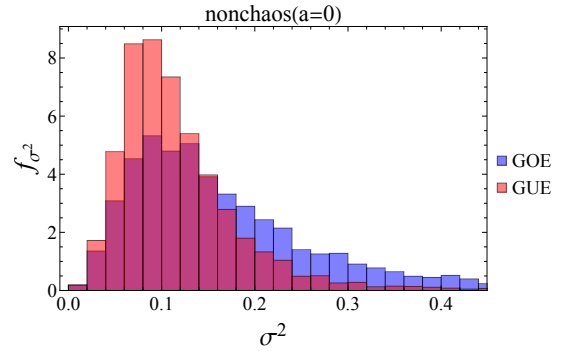


(f) Nonchaotic case $a = 0$ of UCP. Skewness=-0.169296, Kurtosis=3.0196.

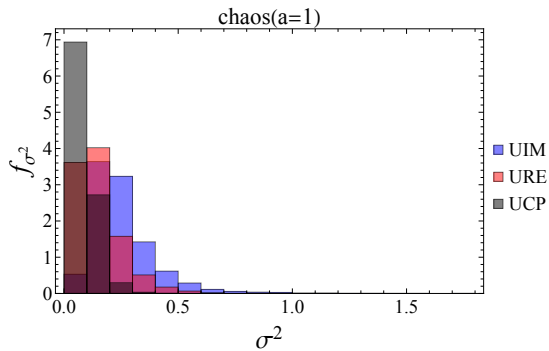
Figure 15: Fitted normal distribution for uniform distributions, $\mathcal{N}_{max} = 100$. The Lanczos coefficients $\{b_n\}$ from step-sizes $1000 \leq n \leq 1500$ are used.



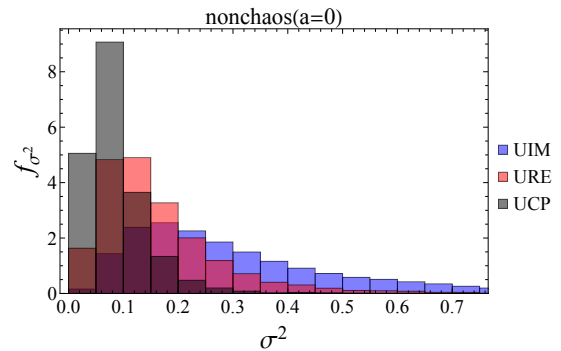
(a) Histogram of σ^2 of GOE and GUE in the chaotic case $a = 1$.



(b) Histogram of σ^2 of GOE and GUE in the nonchaotic case $a = 0$.

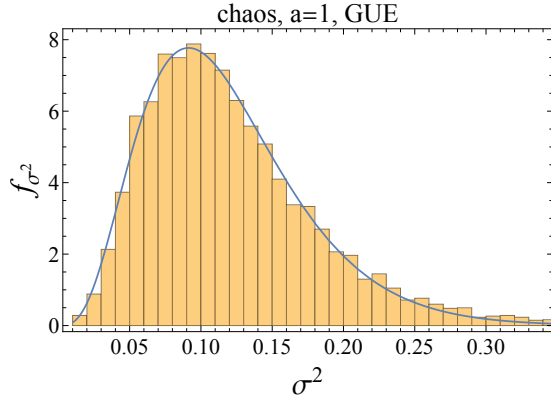


(c) Histogram of σ^2 of uniform distributions in the chaotic case $a = 1$.

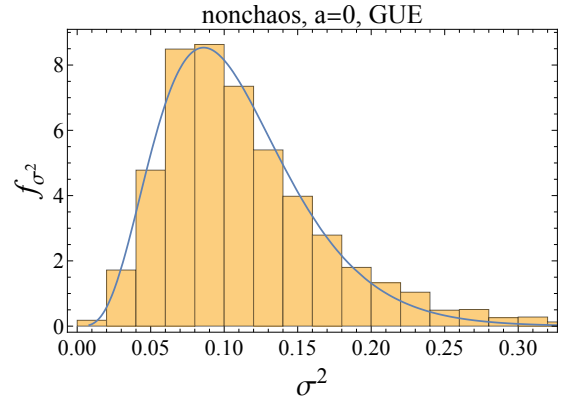


(d) Histogram of σ^2 of uniform distributions in the nonchaotic case $a = 0$.

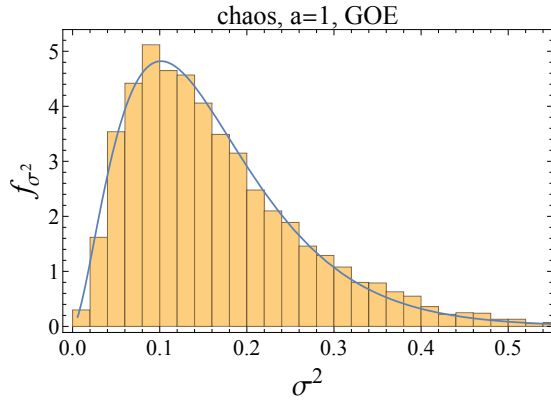
Figure 16: The histogram of variances σ^2 after sampling the initial operator 5000 times from GOE, GUE, URE, UIM and UCP, with $\mathcal{N}_{max} = 5$. Obviously they are not normal distributions.



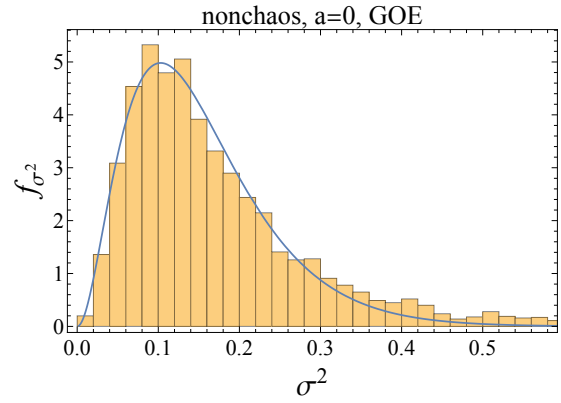
(a) $N = 5$ chaos, GUE. Skewness=1.19843, Kurtosis=5.18562.



(b) $N = 5$ nonchaos, GUE. Skewness=4.30801, Kurtosis=50.7359.

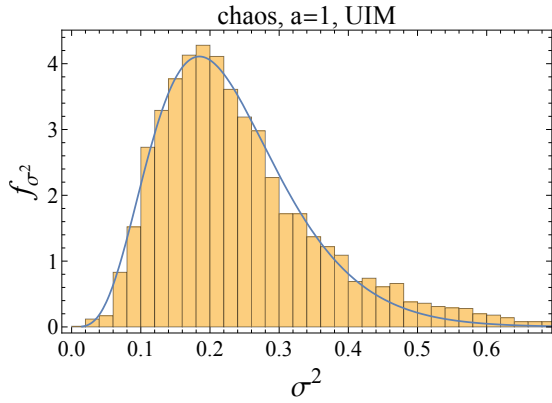


(c) $N = 5$ chaos, GOE. Skewness=1.6231, Kurtosis=7.05429.

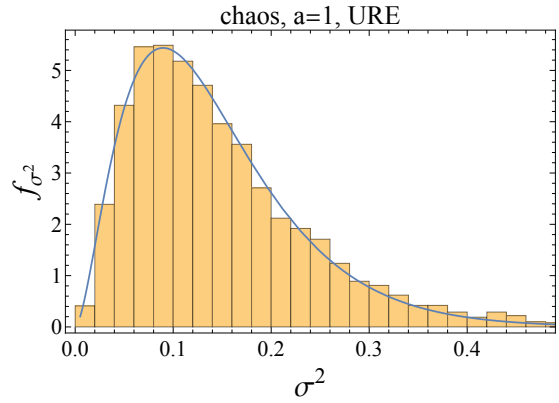


(d) $N = 5$ nonchaos, GOE. Skewness=5.83862, Kurtosis=73.6201.

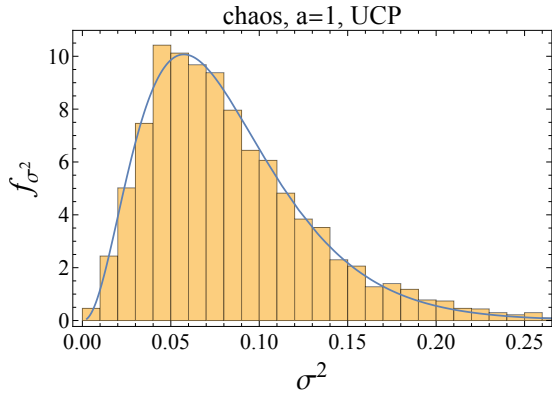
Figure 17: Data fitting of rescaled chi-square distribution for GOE and GUE, $\mathcal{N}_{max} = 5$.



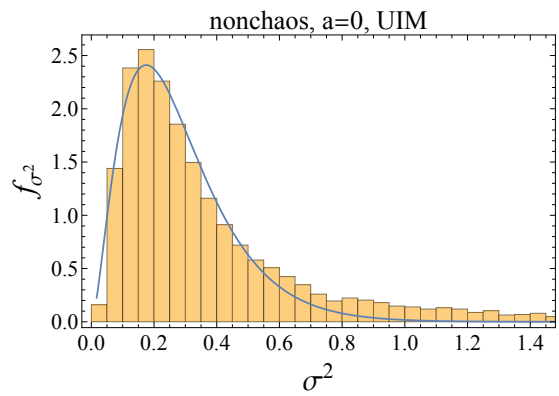
(a) Chaotic case $a = 1$ of UIM. Skewness=0.306957, Kurtosis=3.26486.



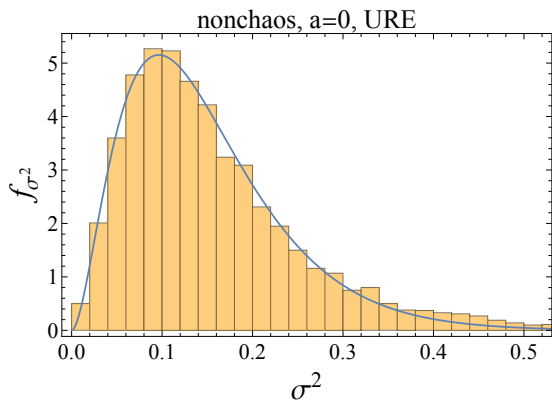
(b) Chaotic case $a = 1$ of URE. Skewness=0.234259, Kurtosis=2.88038.



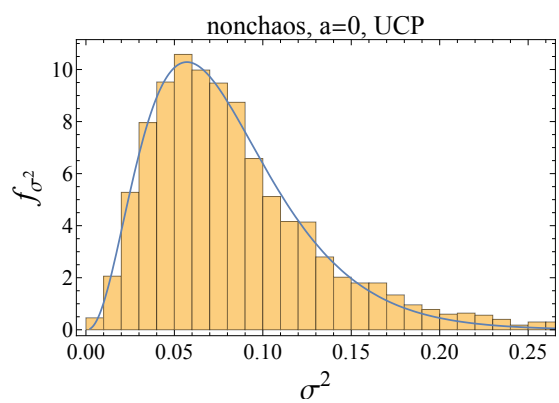
(c) Chaotic case $a = 1$ of UCP. Skewness=0.207669, Kurtosis=2.97609.



(d) Nonchaotic case $a = 0$ of UIM. Skewness=0.0715752, Kurtosis=2.99478.



(e) Nonchaotic case $a = 0$ of URE. Skewness=0.0339498, Kurtosis=3.07535.



(f) Nonchaotic case $a = 0$ of UCP. Skewness=-0.135062, Kurtosis=3.25632.

Figure 18: Data fitting of rescaled chi-square distribution for uniform distributions, $\mathcal{N}_{max} = 5$.

References

- [1] D.E. Parker, X. Cao, A. Avdoshkin, T. Scaffidi and E. Altman, *A Universal Operator Growth Hypothesis*, *Phys. Rev. X* **9** (2019) 041017 [[1812.08657](#)].
- [2] J. Maldacena, S.H. Shenker and D. Stanford, *A bound on chaos*, *JHEP* **08** (2016) 106 [[1503.01409](#)].
- [3] A.I. Larkin and Y.N. Ovchinnikov, *Quasiclassical Method in the Theory of Superconductivity*, *Soviet Journal of Experimental and Theoretical Physics* **28** (1969) 1200.
- [4] F.B. Trigueros and C.-J. Lin, *Krylov complexity of many-body localization: Operator localization in Krylov basis*, *SciPost Phys.* **13** (2022) 037 [[2112.04722](#)].
- [5] E. Rabinovici, A. Sánchez-Garrido, R. Shir and J. Sonner, *Krylov localization and suppression of complexity*, *JHEP* **03** (2022) 211 [[2112.12128](#)].
- [6] E. Rabinovici, A. Sánchez-Garrido, R. Shir and J. Sonner, *Krylov complexity from integrability to chaos*, *JHEP* **07** (2022) 151 [[2207.07701](#)].
- [7] B. Craps, O. Evnin and G. Pascuzzi, *Multiseed Krylov complexity*, [2409.15666](#).
- [8] F.J. Dyson, *Statistical Theory of the Energy Levels of Complex Systems. II*, *Journal of Mathematical Physics* **3** (1962) 157.
- [9] M.C. Gutzwiller, *Periodic orbits and classical quantization conditions*, *J. Math. Phys.* **12** (1971) 343.
- [10] M.V. Berry and M. Tabor, *Level Clustering in the Regular Spectrum*, *Proceedings of the Royal Society of London Series A* **356** (1977) 375.
- [11] O. Bohigas, M.J. Giannoni and C. Schmit, *Characterization of chaotic quantum spectra and universality of level fluctuation laws*, *Phys. Rev. Lett.* **52** (1984) 1.
- [12] R. Blumel and U. Smilansky, *Random-matrix description of chaotic scattering: Semiclassical approach*, *Phys. Rev. Lett.* **64** (1990) 241.
- [13] K. Hashimoto, K. Murata, N. Tanahashi and R. Watanabe, *Krylov complexity and chaos in quantum mechanics*, *JHEP* **11** (2023) 040 [[2305.16669](#)].
- [14] Weinmann, Müller-Groeling, Pichard and Frahm, *$h/2e$ oscillations for correlated electron pairs in disordered mesoscopic rings.*, *Physical review letters* **75** **8** (1995) 1598.
- [15] M. Berry, *Quantizing a classically ergodic system: Sinai's billiard and the kkr method*, *Annals of Physics* **131** (1981) 163.
- [16] P. Nandy, A.S. Matsoukas-Roubeas, P. Martínez-Azcona, A. Dymarsky and A. del Campo, *Quantum Dynamics in Krylov Space: Methods and Applications*, [2405.09628](#).
- [17] M. Mehta, *Random Matrices*, Academic Press (1991).
- [18] A. Dymarsky and A. Gorsky, *Quantum chaos as delocalization in Krylov space*, *Phys. Rev. B* **102** (2020) 085137 [[1912.12227](#)].
- [19] L. Fleishman and D. Licciardello, *Fluctuations and localization in one dimension*, *Journal of Physics C: Solid State Physics* **10** (1977) L125.
- [20] B. Eynard, T. Kimura and S. Ribault, *Random matrices*, [1510.04430](#).
- [21] J. Wishart, *The generalised product moment distribution in samples from a normal multivariate population*, *Biometrika* (1928) 32.

[22] F. Haake, *Quantum signatures of chaos*, Springer (1991).